ChemPubSoc Europe

DOI: 10.1002/chem.201601109

CHEMISTRY A European Journal Full Paper

Photochemistry |*Hot Paper*|

Cooperative Veratryle and Nitroindoline Cages for Two-Photon Uncaging in the NIR

Eduardo Cueto Diaz, Sébastien Picard, Maxime Klausen, Vincent Hugues, Paolo Pagano, Emilie Genin, and Mireille Blanchard-Desce*[a]

Abstract: Tandem uncaging systems in which a two-photon absorbing module and a cage moiety, linked via a phosphorous clip, that act together by Förster resonance energy transfer (FRET) have been developed. A library of these compounds, using different linkers and cages (7-nitroindolinyl or nitroveratryl) has been synthesized. The investigation of their uncaging and two-photon absorption properties demonstrates the scope and versatility of the engineering strategy towards efficient two-photon cages and reveals surprising cooperative and topological effects. The interactions between the 2PA module and the caging moiety are found to promote cooperative effects on the 2PA response while additional processes that enhance the uncaging efficiency are operative in well-oriented nitroindoline-derived dyads. These synergic effects combine to lead to record two-photon uncaging cross-section values (i.e., up to 20 GM) for uncaging of carboxylic acids.

Introduction

Photolabile protecting groups (PPGs) were historically used first by organic chemists and became a valuable tool for applications in multistep organic synthesis, combinatorial chemistry and solid-phase synthesis.[1–6] Several families of such compounds have been described.[7–9] Their key common feature is that they offer protection which is orthogonal to most other protecting strategies as their cleavage requires only light irradiation (classically in the near UV or visible range), without the addition of chemical reagents. Moreover, by using focused light pulses acting as external triggers, PPG removal can be achieved with unique spatial and temporal control. Thanks to these advantages, photosensitive groups have gained increasing popularity in material sciences[10,11] as well as in biology.[2,12,13] Numerous caged proteins and caged biomolecules, the biological activities of which are temporarily masked by the presence of a PPG, have been developed to investigate cellular functions[14–16] or limit toxic effects in drug delivery.[17] The selection of a cage mostly results from a compromise between its characteristics and the requirements dictated by the target application. While systems for photochemical delivery of bioactive volatiles should display slow kinetics to ensure long-lasting effects, time-resolved studies of fast biological processes require PPGs that ensure very fast release and therefore generate a sudden local surge of signaling molecule concentrations. Additional key criteria such as uncaging sensitivity, solubility, dark stability are also to be considered.[7–9] Moreover, enlarging the concept of uncaging to two-photon excitation in the near infrared (NIR) range has been a major breakthrough as it offers intrinsic 3D resolution, reduced out-of-focus damage and improved penetration in tissues.[18,19] This realization initiated the development of specifically designed two-photon sensitive protecting groups combining large two-photon absorption (2PA) cross-section (σ_2) at suitable wavelengths (i.e., in the biological spectral window) with appropriate uncaging quantum yield (Q_u) and thus displaying high 2P uncaging sensitivity (quantified by the 2P uncaging cross-section, $\delta_u = \sigma_2 Q_u$).[20] One of promising ways towards enhanced two-photon sensitivity is based on using well-known protecting groups and embedding them within conjugated dipolar,[21–25] quadrupolar[26–28] and octupolar[29] architectures to improve their 2PA properties. This strategy led in several cases to very interesting cages with δ_u values over 1 GM.[21–28] Yet, a drawback of this strategy is the possible alteration of the uncaging efficiency as a result of the participation of the caging subunit in the intramolecular charge redistribution responsible for large 2PA.[30,31] This may affect the nature of the excited state and lead to a decrease of the uncaging quantum yield as compared to that of the isolated uncaging unit. The outcome of this strategy has appeared to be extremely dependent on the nature of the cage, as well as on the nature and position of the structural modifications. Results are hardly rationalized and this strategy, while being of major interest, remains mostly empirical. Hence, one of the current challenges is the development of versatile and modular routes which could provide more sensitive 2P cages and easily be transposable to different families of PPGs, while retaining their crucial characteristics. Within this context, we focused our efforts on a less-explored

[a] *Dr. E. Cueto Diaz, Dr. S. Picard, M. Klausen, V. Hugues, P. Pagano, Dr. E. Genin, Dr. M. Blanchard-Desce*
University of Bordeaux, Institut des Sciences Moléculaires (UMR5255 CNRS), 351 cours de la liberation, 33450, Talence (France)
E-mail: mireille.blanchard-desce@u-bordeaux.fr

Supporting information for this article is available on the WWW under http://dx.doi.org/10.1002/chem.201601109.

strategy relying on the decoupling between the 2P excitation and uncaging processes.

We recently developed tandem systems[32] where a 2P absorber subunit acts as an intramolecular sensitizer and transfers its excitation energy to the grafted caging unit with the aim to preserve its key chemical (including dark stability) and photochemical (including uncaging kinetics) characteristics. By combining two 7-nitroindolinyl (NI)-caged glutamates with a hydrophilic quadrupolar tailored 2P chromophore, we prepared triads affording a tenfold greater 2P-induced release of glutamate ($\delta_u = 0.5$ GM at 730 nm) in comparison with the parent NI-protecting group. Pursuing the same goal, triads operating by intramolecular electron transfer have been very recently reported as 2P sensitive protecting groups of amino acids with record 2P uncaging sensitivity.[33] Aiming at further increasing the 2PA ability in the 700–800 nm region and assuming that the presence of a second caging unit within the triad could affect the 2P uncaging efficiency of the overall architecture (due to excitation energy trapping by the cage byproduct), we recently[34] elaborated dissymmetric synergic dyads incorporating a nitroveratryl (NV)-derived protecting group. These systems show enhanced σ_2 values (up to 300 GM), sixfold improved 2P uncaging sensitivity in the NIR as well as the possibility to perform 2P photolysis at longer wavelengths (i.e., 800 nm) as compared to the isolated NV cage. Our present goal is to investigate the scope as well as the versatility of our strategy and develop dyads with 2P uncaging sensitivity over 10 GM by using PPGs with larger Q_u values. Herein, we report the synthesis of a series of dyads bearing different 2PA subunits (either pure quadrupoles or slightly dissymmetrized derivatives) shown in Figure 1.

We used linkers of different size and structure enabling the grafting of the caging module to the phosphorus-based clip. We selected either flexible aliphatic spacers (propyle C_3 or hexyle C_6) or semirigid analogues featuring a triazole unit (methyltriazole C_1N_3, propyltriazole C_3N_3, hexyltriazole C_6N_3; Scheme 1 and Scheme 2). In addition to the popular NV caging moiety, NI was selected as a UV absorbing protecting group.

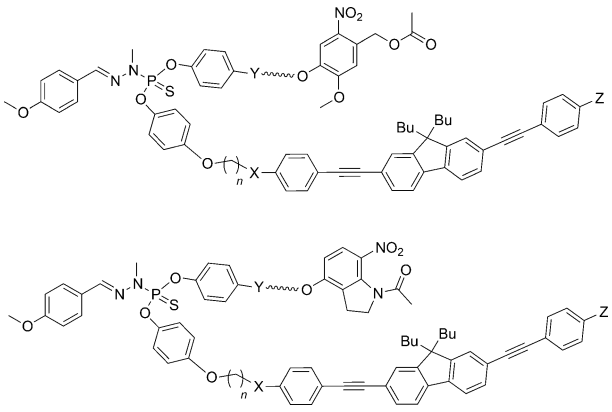

Figure 1. Design of dyads for two-photon induced acetic acid release by combination of a fluorene-cored quadrupolar or dissymmetric two-photon absorber and a caging moiety as 4,5-dimethoxy-2-nitrobenzyl (NV) or 7-nitroindoline (NI).

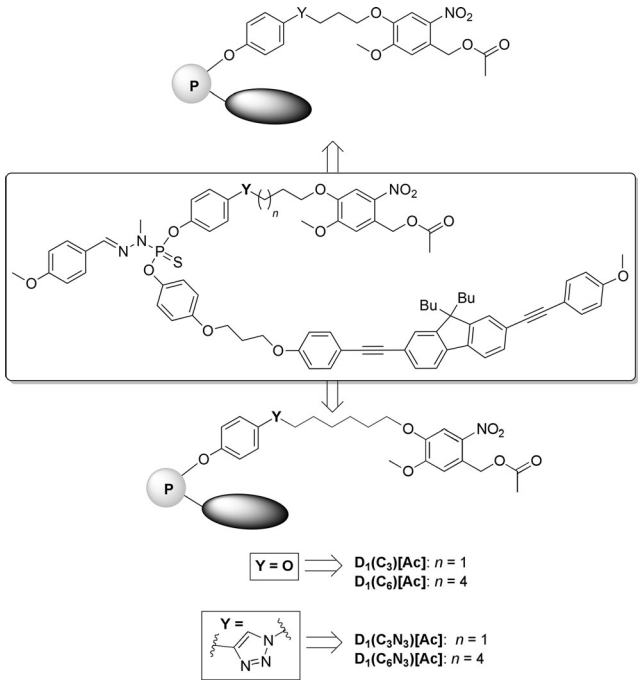

Scheme 1. Schematic representation of a group of dyads having the same sensitizer and caging unit (NV) but different length in the linker.

This choice was motivated by the better (e.g., more than ten-times higher) uncaging quantum yield of NI compared to NV cages as well as key additional features of interest for applications in neurosciences. These include very good dark stability in biological environments and submicrosecond time scale release of neuroactive amino acids such as glutamate or GABA upon flash photolysis[35–38]). These two PPGs display moderate 2P uncaging efficiencies at 730 or 740 nm (δ_u values ranging from 0.03 GM[39] for NV to 0.06 GM[38] for NI) but the NI PPG moiety was quite attractive in view of its use in neurosciences due to the above-mentioned features.

We selected acetic acid as a general model of caged (bio)-molecules featuring a COOH function (including neuro-amino acids). We investigated both the photophysical and 2PA properties of all new dyads as well as their uncaging ability under one-photon excitation in the UV (i.e., 365 nm) and two-photon excitation in a NIR spectral window of interest for biological applications (i.e., 700–1000 nm). This study provides evidence that modulation of the spacer slightly affect the photochemical properties and uncaging sensitivities while the 2PA response of the dyads displays cooperative effect (either positive or negative) depending on the proximity of the polar uncaging moiety to the 2PA module. Importantly, the modification of the PPG (from NV to NI) allows the achievement of a major increase in the uncaging quantum yield. In combination with potentially large 2PA responses, this leads to very large 2P uncaging action cross-section in the NIR region, demonstrating the strength of the implemented engineering strategy.

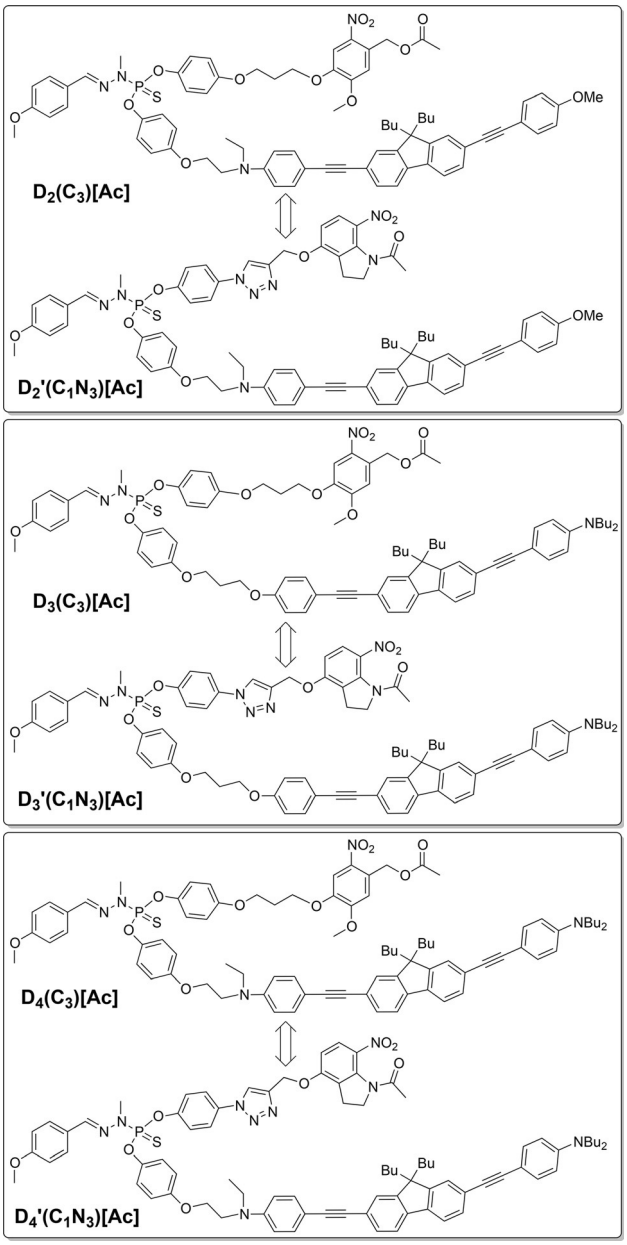

Scheme 2. Comparison of dyads bearing similar sensitizer and linker but different caging units (NV and NI).

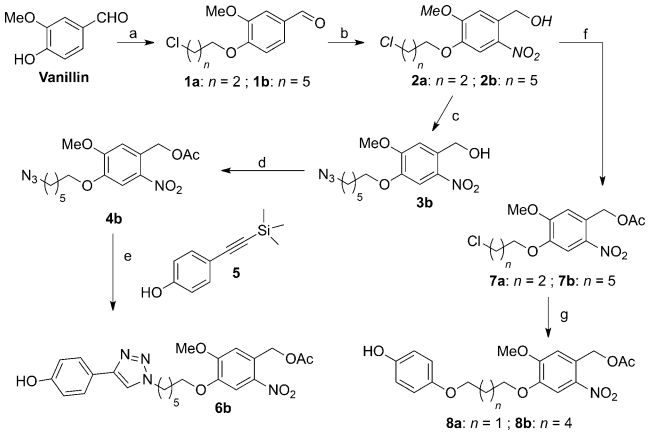

Scheme 3. Synthesis of NV subunits **6** and **8**. Reagents and conditions: a) 1-bromo-3-chloropropane or 1-bromo-6-chlorohexane, K_2CO_3, DMF, RT, overnight (98% of **1a**, 95% of **1b**); b) nitric acid, 0 °C to RT, then $NaBH_4$, methanol or THF, RT, overnight (69% of **2a** and 65% of **2b**); c) NaN_3, DMSO, 70 °C, 4 h (99%); d) Ac_2O, Et_3N, DMAP, CH_2Cl_2, RT, overnight (94%); e) **5**, $CuSO_4 \cdot 5H_2O$, L-ascorbic acid sodium salt, TBAF, DMSO, RT, overnight (70%); f) Ac_2O, DMAP, Et_3N, CH_2Cl_2, RT, overnight (95% of **7a**, 99% of **7b**); g) NaI, acetone, 60 °C, 2 days, then hydroquinone, K_2CO_3, DMF, 40 °C, 36 h (51% of **8a**, 47% of **8b**).

Results and Discussion

Synthesis of the graftable subunits

The synthesis of the graftable 6-nitroveratryl acetate subunit **6** bearing a hexyltriazole spacer was achieved by adapting the synthetic route recently reported for the preparation of the analogue with a shorter propyltriazole linker.[34] The NV derivative **6** was obtained in six steps starting from vanillin in a satisfactory 40% overall yield (Scheme 3). Alkylation of vanillin with either 1-bromo-3-chloropropane or 1-bromo-6-chlorohexane in the presence of anhydrous potassium carbonate in DMF afforded compounds **1a**[34] and **b** in almost quantitative yields. The nitration of benzaldehydes **1a**–**b** with nitric acid followed by the reduction of the aldehyde group provided alcohols **2a**[34] and **b** efficiently. Nucleophilic substitution of the chlorine with sodium azide led to compound **3** which was subsequently treated with acetic anhydride to afford the benzylic ester **4** with an excellent yield. Finally, the introduction of the phenol terminal grafting moiety was achieved using a one-pot two-step protocol involving the in situ deprotection of the TMS-protected alkyne **5**[34] followed by a Huisgen 1,3-dipolar cycloaddition with azide **4** and the NV-caged acetate module **6** was isolated in 70% yield.

The graftable NV derivatives **8a** and **8b**, bearing propyl and hexyl spacers, respectively, were obtained from the key intermediates **2a** and **2b** in a two-step sequence. Esterification with acetic anhydride afforded compounds **7a**[34] and **b** with a chlorine extremity. Following this second route, the introduction of the phenol terminal grafting moiety was achieved by means of a nucleophilic substitution with hydroquinone which led to **8a**[34] and **b** in moderate yields. The NI-based (**14**) caging module featuring a phenol pendant moiety were prepared in four steps, from the known *N*-acetyl-4-hydroxyindoline (**9**) derivative (Scheme 4). Protection of the phenol group by using *tert*-butyldimethylsilyl chloride afforded compound **10**. A nitration reaction under mild conditions in the presence of copper nitrate[40] was subsequently performed to obtain a mixture of both 5- and 7-nitro regioisomers **11a** and **11b**. These products were separated by column chromatography on silica gel, thus yielding **11a** and **11b** as pure regioisomer compounds. The 7-nitro isomer **11b** was converted to the corresponding propargylated derivative **12** by means of a silyl group deprotection reaction followed by propargylation. Applying a one-pot procedure, **11b** was therefore treated with tetra-*n*-butylammonium fluoride (TBAF) and the resulting unstable phenolate was treated in situ with propargyl bromide to

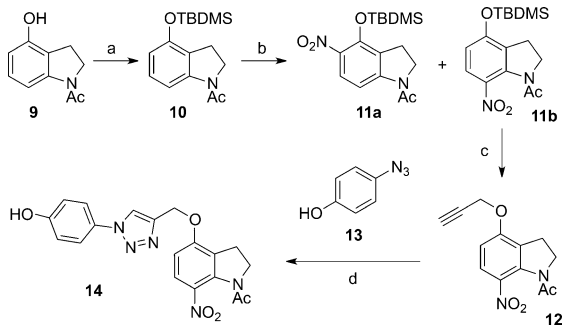

Scheme 4. Synthesis of **MNI14**. Reagents and conditions: a) TBDMSCl, imidazole, DMF, RT, overnight (96%); b) $Cu(NO_3)_2{\cdot}3H_2O$, CH_2Cl_2/Ac_2O, RT, overnight (26% of **11a**, 28% of **11b**); c) propargyl bromide, KI, TBAF, THF, RT, overnight (93%); d) L-ascorbic acid Na salt, $CuSO_4{\cdot}5H_2O$, DMSO, RT, overnight (92%).

give **12** with excellent yield. Huisgen 1,3-dipolar cycloaddition with 4-azidophenol[41] **13** provided the graftable NI subunit **14**.

The synthesis of the graftable dissymmetric two-photon absorbing modules $\mathbf{M_{1-4}}$ (Scheme 5) was achieved by stepwise functionalization of a diidofluorene core involving an in situ deprotection/double Sonogashira coupling protocol, as we recently reported (see the Supporting Information for the synthesis of $\mathbf{M_4}$).[34,42,43] All synthetic intermediates as well as graftable subunits were fully characterized by ^1H and ^{13}C NMR spectroscopy and mass spectrometry.

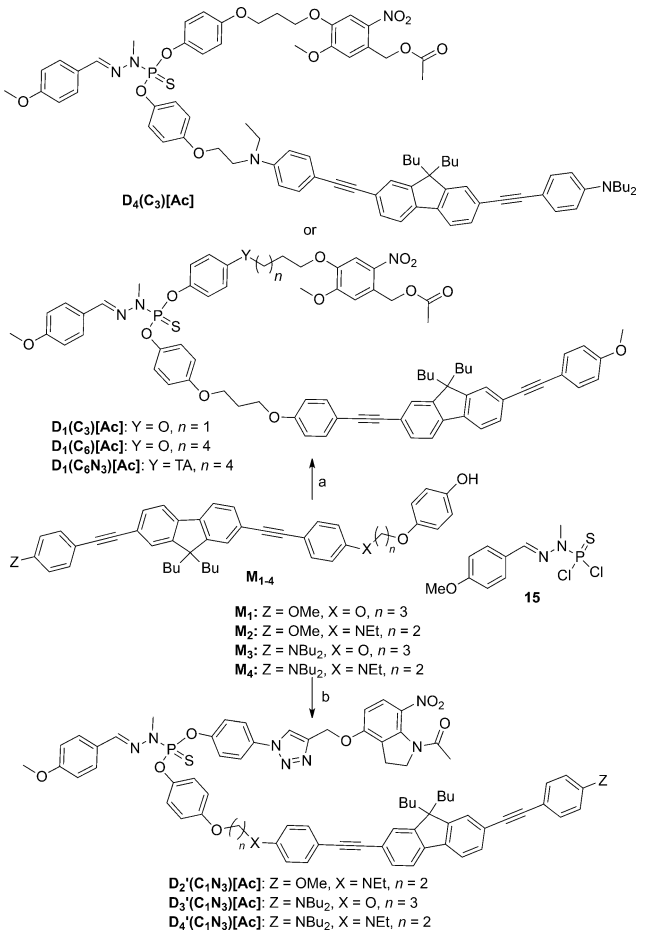

Scheme 5. Synthesis of dyads. Reagents and conditions: a) **6** or **8a**–**b**, **15**, Cs_2CO_3, THF, RT, 16 h and then $\mathbf{M_1}$ or $\mathbf{M_4}$, THF, RT, 18 h (8% for $\mathbf{D_1(C_3)[Ac]}$, 12% for $\mathbf{D_1(C_6)[Ac]}$, 24% for $\mathbf{D_1(C_6N_3)[Ac]}$, 59% for $\mathbf{D_4(C_3)[Ac]}$); b) **14**, **15**, Cs_2CO_3, THF, RT, 16 h and then $\mathbf{M_2}$, $\mathbf{M_3}$ or $\mathbf{M_4}$, THF, RT, 18 h (23% for $\mathbf{D_2'(C_1N_3)[Ac]}$, 28% for $\mathbf{D_3'(C_1N_3)[Ac]}$, 25% for $\mathbf{D_4'(C_1N_3)[Ac]}$).

Synthesis of the synergic dyads

The preparation of the small library of synergic structures bearing various absorbing and caging modules is depicted in Scheme 5. Taking advantage of the efficient nucleophilic substitutions of the chlorine atoms in the $P(S)Cl_2$ moiety, by phenolic derivatives, the synthetic pathway was based on the sequential functionalization of the clipping scaffold **15**.[34] Importantly, the mono-functionalization of only one P–Cl bond among the two is possible thanks to the significantly lower reactivity of the P(S)(OAr)Cl moiety compared to $P(S)Cl_2$. To prepare dyads featuring NV and NI moieties, we then applied a two-step one-pot procedure involving first the coupling of **15** with a stoichiometric amount of caging subunits **6** or **8a**–**b** or **14**, followed by the substitution of the remaining Cl in the presence of the phenolic anion of chromophoric subunits $\mathbf{M_{1-4}}$.

The synthesis of the dyads was conducted in the dark at room temperature under inert atmosphere. A THF solution of one equivalent of the graftable caging module was added dropwise to a THF solution containing the phosphorus-based clip **15** and cesium carbonate. The reaction proceeded smoothly in few hours and the reaction progress was monitored by ^{31}P and ^1H NMR spectroscopy. The completion of the first step was demonstrated by the appearance of a singlet at approximately 69 ppm in the ^{31}P spectrum attributed to the P(S)(OAr)Cl group (Figure 2).

The completion of the first step was further confirmed by the disappearance of the signals corresponding to the phenol moiety of the starting material **6** or **8a**–**b** or **14** in the ^1H NMR spectrum. A THF solution of the graftable 2PA module $\mathbf{M_{1-4}}$ was then added dropwise to the reaction mixture in order to substitute the second P–Cl bond. Once again, ^{31}P NMR spectroscopy was an invaluable tool for monitoring the reaction progress. The total disappearance of the signal at approximately 69 ppm and appearance of a more shielded singlet at 63.8 ppm proved the completion of the second step after 18 h (Figure 2). Cesium salt residues were removed by centrifugation of the reaction mixture. The $\mathbf{D_1}$ series of dyads with alkyl or hexyltriazole spacers as well as dyads $\mathbf{D_{2-4}'}$ incorporating an NI-caged acetate were then obtained with moderate yields as pure compounds after column chromatography (which leads to loss of compound explaining the modest yield in purified dyads). Characterization by ^1H and ^{31}P NMR spectroscopy and MALDI-TOF mass spectrometry unambiguously proved the structure and the high purity of all the synthesized dyads.

Photophysical and two-photon absorption properties

The photophysical and two-photon absorption (2PA) properties of the dyad compounds were investigated in chloroform and the corresponding data are gathered in Table 1. For the

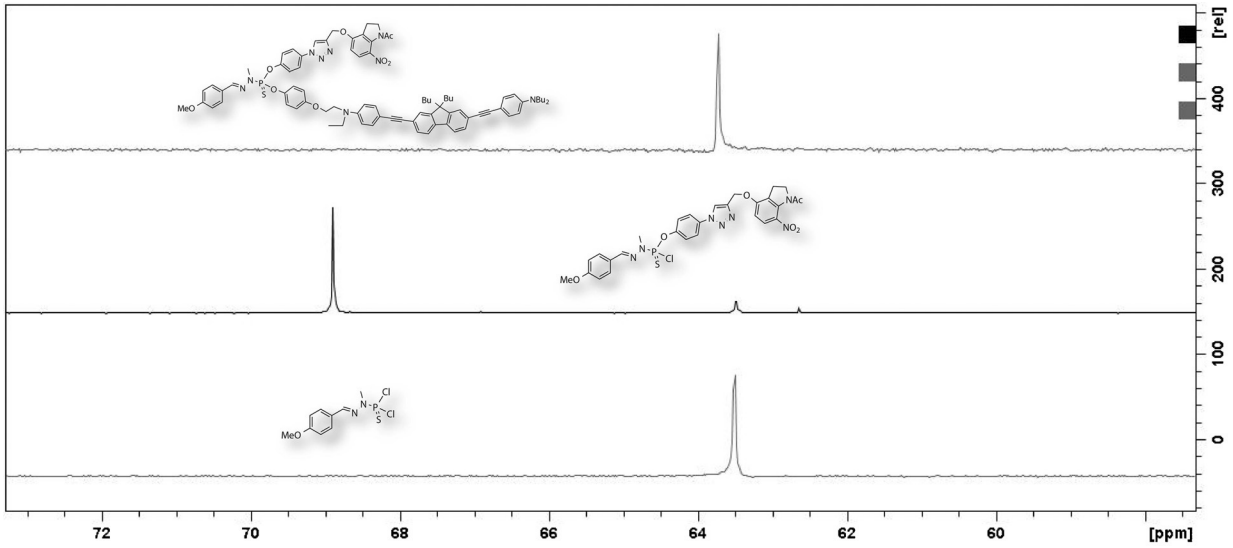

Figure 2. ^{31}P NMR monitoring in $CDCl_3$ of the synthesis of the **$D_3'(C_1N_3)$[Ac]**: dyad: spectrum of **15** (bottom); spectrum of the reaction mixture **15** and **14** (middle); spectrum of the **$D_3'(C_1N_3)$[Ac]** synergic dyad (top).

sake of comparison, the characteristics of the 2PA modules are also included.

Photophysical properties

The 2PA modules as well as the dyads display an intense absorption band in the near-UV region with maximum molar extinction coefficient values ranging from 6.5 to $9.0\times10^4\,M^{-1}\,cm^{-1}$, which are at least tenfold larger than that of the NV and NI cages. The isolated 2PA modules show intense fluorescence emission in the near-UV–blue visible region with large fluorescence quantum yields ($\approx$0.70). As anticipated, a bathochromic shift of both the absorption and emission bands is observed when the strength of the electron-releasing end-group increases. Importantly, the superimposition of the emission spectra of the 2PA modules **M_1**–**M_4** with the absorption spectra of the NV and NI cages highlights overlaps (Figure 3) which markedly decrease on going from **M_1** to **M_2**, **M_4** and **M_3**, thus suggesting that resonant-energy transfer from **M_1** modules to the close NV or NI cages should be more efficient. This trend is confirmed when comparing the fluorescence quantum yields of isolated 2PA modules and those of the corresponding dyads. Indeed, dyads **D_1**, bearing **M_1** as a 2PA module, show a marked fluorescence quantum yield reduction (varying between 45 and 30% depending on the nature of the linker between 2PA modules and uncaging moiety). In contrast dyads **D_2**, **D_3** and **D_4** having **M_2**, **M_3** and **M_4** two-photon absorbing modules show smaller fluorescence

Table 1. Photophysical data of dyads and of their corresponding 2PA subunit and uncaging modules in $CHCl_3$.

Cpd	λ_{abs}^{max} [nm]	ε^{max} [$M^{-1}\,cm^{-1}$]	ε_{365nm} [$M^{-1}\,cm^{-1}$]	λ_{em}^{max} [nm]	Φ_f[a]	Q_u/Q_u^{ref}	$\varepsilon^{max}Q_u$ [$M^{-1}\,cm^{-1}$][b]	$2\lambda_{abs}^{max}$ [nm]	λ_{2PA}^{max} [nm]	σ_2^{max} [GM][c]	δ_u [GM][d]
NVOAc	341	5.9×10^3	4.0×10^3	–	–	1	35			–	0.03[e]
MNI	302	4.8×10^3	1.9×10^3	–	–	1	384			–	0.06[f]
M_1	358	7.2×10^4	6.6×10^4	384	0.70	–	–	716	720	30	–
$D_1(C_3)$[Ac]	358	7.5×10^4	6.8×10^4	383	0.41	0.32	146	716	730	55	0.11
$D_1(C_3N_3)$[Ac][34]	358	9.0×10^4	7.2×10^4	383	0.45	0.36	197	716	730	50	0.11
$D_1(C_6)$[Ac]	358	8.1×10^4	7.4×10^4	383	0.49	0.36	174	716	730	45	0.10
$D_1(C_6N_3)$[Ac]	358	8.3×10^4	7.5×10^4	383	0.38	0.26	128	716	730	30	0.05
M_2	368	7.8×10^4	7.7×10^4	435	0.69	–	–	736	750	195	–
$D_2(C_3)$[Ac][34]	367	7.6×10^4	7.6×10^4	433	0.57	0.11	48	734	750	160	0.10
$D_2'(C_1N_3)$[Ac]	367	6.9×10^4	6.9×10^4	434	0.58	0.26	1510	734	770	170	3.7
M_3	375	6.5×10^4	6.1×10^4	446	0.65	–	–	750	800	240	–
$D_3(C_3)$[Ac][34]	373	6.8×10^4	6.5×10^4	446	0.57	0.13	55	746	800	310	0.25
$D_3'(C_1N_3)$[Ac]	375	6.5×10^4	6.2×10^4	446	0.57	0.09	490	750	800	300	2.3
M_4	385	7.9×10^4	5.6×10^4	431	0.75	–		770	710	1370	
$D_4(C_3)$[Ac]	386	7.0×10^4	5.4×10^4	431	0.65	0.13	53	772	710	1300	0.98
$D_4'(C_1N_3)$[Ac]	386	7.1×10^4	5.4×10^4	431	0.67	0.19	1130	772	710	1270	20

[a] Fluorescence quantum yield, standard: quinine in 0.5 M H_2SO_4 ($\Phi=0.546$). [b] One-photon uncaging sensitivity derived from comparative one-photon photolysis experiments at 365 nm, using $Q_u=0.006$ for NVOAc and $Q_u=0.08$ for MNI. [c] Two-photon absorption cross-section at λ_{2PA}^{max} derived from TPEF experiments (1 GM = 10^{-50} $cm^4\,s^{-1}$). [d] Two-photon uncaging sensitivity ($\delta_u=\sigma_2^{max}Q_u$) [e] From reference [39] at 740 nm, [f] From reference [38] at 730 nm.

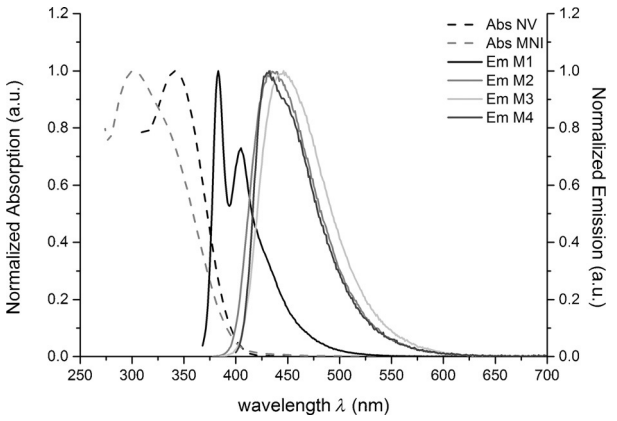

Figure 3. Normalized absorption spectra of NV and NI cages and emission spectra of 2PA chromophores $\mathbf{M}_{1-4}$ in chloroform.

quantum yield decrease (16–17% for dyads $\mathbf{D}_2$ and $\mathbf{D}_2'$, 11–13% for dyad $\mathbf{D}_4$ and $\mathbf{D}_4'$ and 12% for dyads $\mathbf{D}_3$ and $\mathbf{D}_3'$) which is consistent with the decreasing overlap of the absorption spectrum of the acceptor (NV or NI) and emission of the donor (i.e., $\mathbf{M}_2$, $\mathbf{M}_4$, $\mathbf{M}_3$).

It is interesting to note that the $\mathbf{M}_3$ 2PA module, though displaying blue-shifted absorption as compared to $\mathbf{M}_4$, shows red-shifted emission, thus leading to slightly smaller overlaps. This might be related to the intrinsic electronic dissymmetry of the $\mathbf{M}_3$ module compared to $\mathbf{M}_4$. This dissymmetry promotes symmetry breaking in the excited state leading to more polar excited states which are stabilized in medium to high polarity environments, leading to a red-shifted emission.[44]

Comparison of $\mathbf{D}_1$ dyads, bearing the $\mathbf{M}_1$ 2PA module, shows that the length and nature of the linker between the 2PA and uncaging subunits slightly influence their photochemical behavior. In the case of aliphatic linkers, the shortest linker seems to lead to the most pronounced decrease of the fluorescence quantum yield (see comparison of **$\mathbf{D}_1$($\mathbf{C}_3$)[Ac]** and **$\mathbf{D}_1$($\mathbf{C}_6$)[Ac]** dyads). On the other hand the presence of the triazole moiety in the linker seems to have a distinct influence. Indeed **$\mathbf{D}_1$($\mathbf{C}_3\mathbf{N}_3$)[Ac]** dyad shows a slightly more pronounced fluorescence reduction than dyad **$\mathbf{D}_1$($\mathbf{C}_6$)[Ac]** (36 versus 30%), although the length of their spacers are similar. Additionally, **$\mathbf{D}_1$($\mathbf{C}_6$)[Ac]** dyad which has the longest spacer shows the largest fluorescence quenching which amounts up to 46%. This unusual observation points to the possible role of the triazole moiety as a passive chromophore mediating resonant-energy transfer between the 2PA module and uncaging moieties.[45] Finally, we observe that dyads $\mathbf{D}_2$ and $\mathbf{D}_2'$ as well as $\mathbf{D}_3$, $\mathbf{D}_3'$ and $\mathbf{D}_4$, $\mathbf{D}_4'$ show a similar fluorescence decrease as expected from the overlap between $\mathbf{M}_2$–$\mathbf{M}_4$ in the emission spectrum and the NV and MNI absorption spectra (Figure 3).

Two-photon absorption properties

Both 2PA modules and corresponding dyads display a broad 2PA band in the NIR region the intensity of which strongly depends on the nature of the 2PA module (Table 1 and the Supporting Information).

Only $\mathbf{M}_1$ and $\mathbf{M}_4$ are essentially quadrupolar in nature. Hence, their 2PA response at twice the maximum (one-photon) absorption wavelength is rather modest (Table 1) in relation with the fact that the lowest excited is strongly one-photon allowed but almost two-photon forbidden. The higher energy, strongly two-photon allowed, excited state is clearly observed for $\mathbf{M}_4$ (at 710 nm) while it falls out of the NIR range in the case of $\mathbf{M}_1$ (i.e., at $\lambda_{2PA} < 700$ nm). Conversely, $\mathbf{M}_2$ and $\mathbf{M}_3$ are not purely quadrupolar as they bear two different electron-donating end-groups, thus relieving the symmetry interdiction for 2PA to the lowest excited state. As a result, both show significant 2PA responses in the 750–800 nm spectral range corresponding to the transition to the lowest (strongly one-photon allowed) excited state, with respective maxima located at 750 and 800 nm, and corresponding σ_2^{max} values of, respectively, approximately 160 GM and about 300 GM (Table 1). Quite interestingly, we observe that the close proximity between the uncaging (NV or MNI) moiety and 2PA modules ($\mathbf{M}_1$–$\mathbf{M}_4$) influences their 2PA response.

Comparison of the 2PA spectra of the series of $\mathbf{D}_1$ dyads with that of their 2PA module indeed demonstrates the influence of the proximity of the uncaging moiety on the dyads 2PA response (Figure 4). The presence of the uncaging moiety increases the maximum 2PA response in the 700–1000 nm

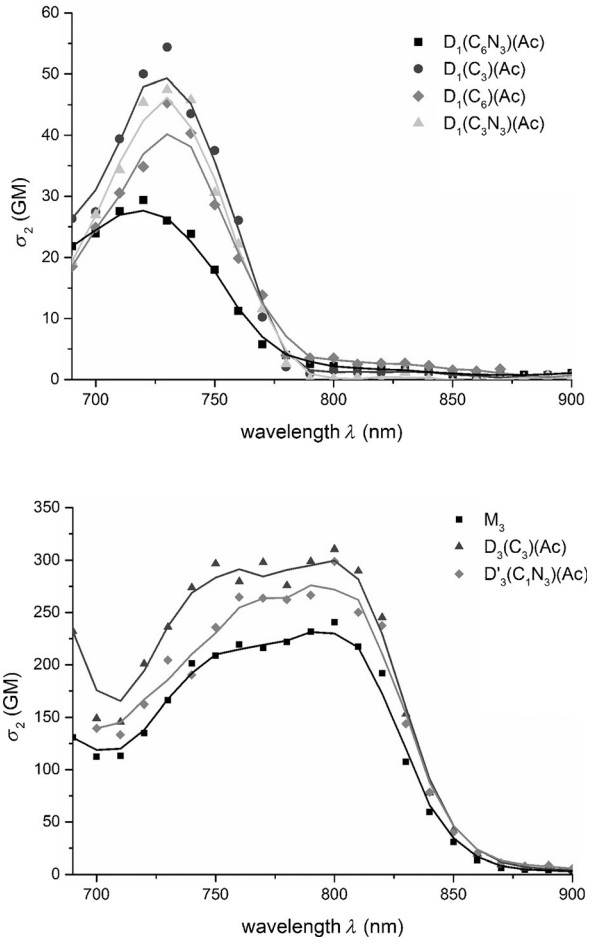

Figure 4. Two-photon absorption spectra of $\mathbf{D}_1$ dyads (top) and $\mathbf{D}_3$-$\mathbf{D}_3'$dyads (bottom) compared to their 2PA module ($\mathbf{M}_3$).

spectral range (i.e., biological window) by up to 85% (Table 1). We note that this effect decreases with increasing distance between the uncaging and 2PA module being maximum for the **$D_1(C_3)$[Ac]** dyad (in which the two modules are the closest) and vanishing for the **$D_1(C_6N_3)$[Ac]** dyad having the longest spacer. This can possibly be related to the effect of the electrostatic electric field generated by the dipolar uncaging moiety (thus depending markedly on proximity) on the 2PA module. Previous reports have shown that the two-photon absorption response of both dipolar and quadrupolar chromophores can indeed be influenced by electrostatic interactions.[43,46] As a consequence the **$D_1(C_3)$[Ac]** dyad shows a maximum 2PA cross-section value at 720 nm which, while modest, is still more than one order of magnitude larger than that of the isolated NV cage. Hence, the dyad strategy also provides an indirect way to enhance the 2PA response by taking advantage of the dipolar nature of uncaging moieties and electrostatic effects.

We also observe a definite effect of the spatial proximity between uncaging moieties and 2PA on the 2PA responses of dissymmetric dyads **D_2-D_2′** and **D_3-D_3′**. Quite interestingly, a decrease of the 2PA response by about 15% is observed for **D_2-D_2′** dyads compared to their 2PA module **M_2**, whereas an increase of 27% is observed for **D_3-D_3′** dyads (Figure 4 and Table 1). This reverse trend can be related to the opposite orientation of the resulting dipole of the dissymmetric 2PA module **M_2** and **M_3** with respect to the caging dipolar moieties. **D_4-D_4′** dyads display an intermediate behavior with only a very slight decrease of the peak 2PA response (Table 1 and the Supporting Information).

One- and two-photon uncaging studies

One-photon uncaging properties

The uncaging properties of the dyads were first investigated by performing one-photon photolysis of samples in $CDCl_3$ upon excitation at 365 nm. For direct comparison, photolysis of the isolated NV and NI-caged acetate were also carried out in the same experimental conditions (i.e., at the same absorbance at 365 nm and the same excitation power).

The time courses for the photolysis reactions were monitored by ^{1}H NMR analysis. The production of the photoreleased acetic acid was evidenced by the onset of a singlet at 2.10 ppm (δCH_3), while the signal of the caged acetyl group at 2.16 or 2.23 ppm (δCH_3), in the case of NV and MNI-based dyads, respectively, concomitantly vanished. Quantitative analysis of the amount of photoreleased acetic acid allowed the plotting of the conversion rate over time. All derivatives display first-order kinetics profiles from which the corresponding slope values (photolysis rate constants) could be derived (Figure 5 and Figure 6). Comparison of the slope values, which are proportional to $\varepsilon_{(365nm)}Q_u$, provided relative Q_u values for each dyad with respect to that of the corresponding isolated caging moiety (Q_u/Q_u^{ref} values reported in Table 1). One-photon uncaging sensitivities of dyads were then calculated from the Q_u values reported in the literature for NV[39] (0.006), MNI[38] (0.08) cages.

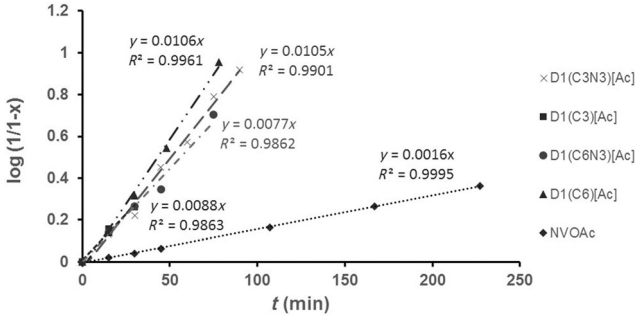

Figure 5. Kinetics of acetic acid photorelease induced upon irradiation at 365 nm for the series of **D_1**-based dyads and the reference NVOAc cage.

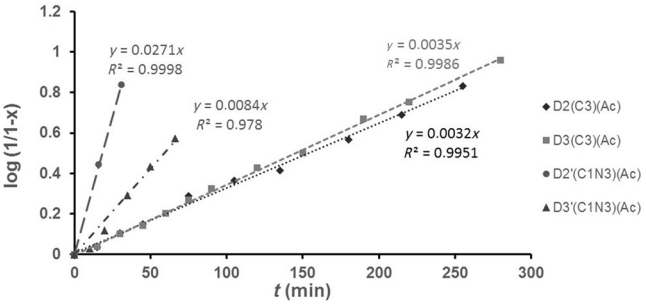

Figure 6. Comparison of the kinetics of acetic acid photoinduced release (upon irradiation at 365 nm) between NV- and MNI-derived dyads.

As seen from Table 1, the length and the nature of the spacer are found to slightly affect the uncaging sensitivity of the series of **D_1** dyads (Figure 5). **$D_1(C_6N_3)$[Ac]** dyad displays the lowest relative Q_u ratio (0.26), while **$D_1(C_3N_3)$[Ac]** and **$D_1(C_6)$[Ac]** exhibit the highest Q_u ratio value (0.36). This suggests an optimum linker length that leads to the highest uncaging quantum yield. As a result, the one-photon uncaging sensitivities (i.e., $\varepsilon^{max}Q_u$) of **D_1** dyads are thus enhanced by a factor 4 to 6 in comparison with NVOAc (Table 1). In contrast **D_2**, **D_3** and **D_4** dyads show lower relative Q_u ratio values than **D_1** dyads, in agreement with the smaller overlaps between the NV absorption spectrum and the different 2PA modules (**M_{2-4}**) emission spectra.

As a result **D_2**, **D_3** and **D_4** dyads show one-photon uncaging sensitivities which are only slightly larger than that of NVOAc (Table 1). On the other hand, we observe that **D_2′**, **D_3′** and **D_4′** dyads undergo much faster one-photon photolysis at 365 nm compared to their NV-bearing counterparts (Figure 6 and the Supporting Information). This demonstrates the scope of the implemented strategy in terms of sensitizing various cages. Indeed by using more efficient (i.e., having larger uncaging quantum yield) cages such as NI, dyads with larger uncaging sensitivities are achieved (typically from 500 to 1500 $M^{-1}cm^{-1}$, which is fourfold larger than that of isolated MNI). Quite interestingly, we notice that the Q_u ratio values are different for the analogous NV and MNI dyads. Indeed **D_2′(C_1N_3)[Ac]** and **D_4′(C_1N_3)[Ac]** dyads display significant Q_u ratio values (0.26 and 0.19)—larger than that of **$D_2(C_3)$[Ac]** and **$D_4(C_3)$[Ac]** dyads—despite the very small spectral overlap between absorption of NI

and emission of $\mathbf{M_2}$ and $\mathbf{M_4}$. In contrast, $\mathbf{D_3'(C_1N_3)[Ac]}$ dyad shows a low Q_u ratio value (0.09), slightly smaller than that of $\mathbf{D_3(C_3)[Ac]}$. Hence, the Q_u ratio value increases for the $\mathbf{D_2'}$ dyad as compared to the $\mathbf{D_2}$ dyad whereas it slightly decreases for the $\mathbf{D_3'}$ dyad as compared to the $\mathbf{D_3}$ dyad. This singular behavior suggests that additional processes contribute to the uncaging mechanism in the case of $\mathbf{D_2'}$ and $\mathbf{D_4'}$ dyads. This could be related in particular to triplet–triplet sensitization (as reported earlier in the case of NI-derived dyads[47]) or to electron transfer mediated uncaging.[33,48,49] The contribution of electron transfer from the excited 2PA module to the MNI moiety might be significant in particular within $\mathbf{D_4'}$ ($\mathbf{M_4}$ having the strongest electron-donating end-groups)[33] as well as for the $\mathbf{D_2'}$ dyad (where electron transfer is favored from a topological point of view, due to the closer proximity of the strongest electron-donating end-group).

As a consequence, the one-photon uncaging sensitivity ($\varepsilon^{max}Q_u$) of $\mathbf{D_2'(C_1N_3)[Ac]}$ shows a 30-fold enhancement compared to $\mathbf{D_2(C_3)[Ac]}$ and that of $\mathbf{D_4'(C_1N_3)[Ac]}$ a 20-fold enhancement compared to $\mathbf{D_4(C_3)[Ac]}$ while $\mathbf{D_3'(C_1N_3)[Ac}$ shows only a ninefold enhancement compared to $\mathbf{D_3(C_3)[Ac]}$. This markedly different enhancement factor clearly emphasizes the role of the topology of the dyads in triggering cooperative effects on uncaging efficiency of the NI cage.

Two-photon uncaging properties

Maximum 2P uncaging action cross-sections ($\delta_u = \sigma_2^{max} Q_u$) were then derived for all dyads from the experimentally determined σ_2^{max} and Q_u values, assuming that one-photon and two-photon uncaging quantum yields are the same (Table 1).

Except for the twofold less sensitive $\mathbf{D_1(C_6N_3)[Ac]}$ derivative, $\mathbf{D_1}$-based dyads have threefold larger 2P uncaging sensitivities ($\approx$0.10 GM at 730 nm) compared to the NV reference, whatever the spacer featured. This results from the variation of the 2PA responses which compensates for the variation of the uncaging quantum yields. As previously reported, $\mathbf{D_2}$-$\mathbf{D_3}$ dyads show larger 2P uncaging sensitivities (up to 0.25 GM).[34] Notably, the $\mathbf{D_4}$ dyad shows a larger 2P uncaging sensitivity (i.e., 1 GM), leading to the most efficient uncaging system among the NV-derived dyads.

More importantly, replacing the NV unit by an NI caging moiety having a tenfold larger uncaging quantum yield led to a major increase in the 2P uncaging cross-sections. $\mathbf{D_2'(C_1N_3)[Ac]}$, $\mathbf{D_3'(C_1N_3)[Ac]}$ and $\mathbf{D_4'(C_1N_3)[Ac]}$ dyads were found to be up to more than two orders of magnitude more sensitive than the NI reference, thus affording large δ_u values of, respectively, 3.7 GM (at 770 nm), 2.3 GM (at 800 nm) and 20 GM (at 710 nm). In particular, the $\mathbf{D_4'(C_1N_3)[Ac]}$ dyad, which benefits both from the strongly two-photon allowed transition at 710 nm and significant uncaging quantum yield (in relation with the contribution of different mechanisms in addition to FRET) show the highest two-photon uncaging cross-section. To the best of our knowledge, this record value overcomes those reported up to now for most functional uncaging systems for the release of acids, opening a new avenue for uncaging applications in neurosciences.

Based on these results, 2P photolysis experiments were conducted with the NI-derived dyads which show large 2P uncaging action cross-sections. Namely, the dyads were dissolved in $CDCl_3$ and irradiated at wavelengths corresponding to maximum 2PA responses within the spectral range of interest for biological applications (690–1000 nm) using a Ti-sapphire laser delivering 140 fs pulses at 80 MHz repetition rate. After few hours of irradiation (this typical duration is required due to the extremely small fraction of the total volume of the cuvette (mL) addressed with highly confined two-photon excitation), the production of 2P photoreleased acetic acid was assessed by ^{1}H NMR analysis (Figure 7 and the Supporting Information). Due to the experimental conditions (total volume, high repetition rate of the fs laser and duration of the experiment), the observed kinetics of the overall process depends both on the

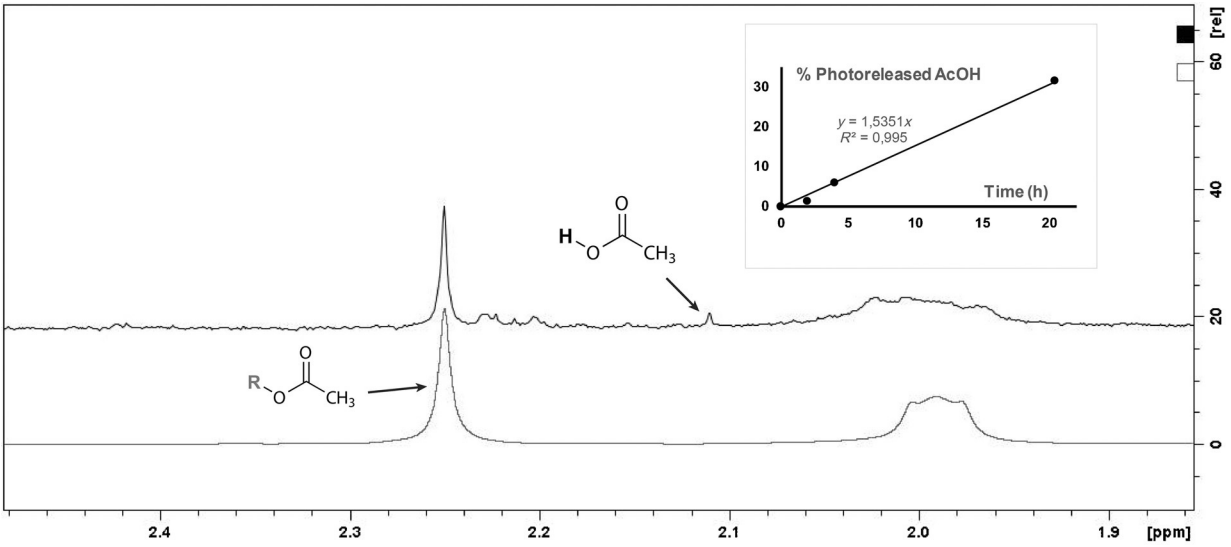

Figure 7. ^{1}H NMR spectrum (300 MHz) of $\mathbf{D_4'(C_1N_3)[Ac]}$ in $CDCl_3$ at $t = 0$ (bottom) and after 4 h two-photon irradiation at 720 nm (top).

2P-uncaging action cross-section (which influences the photolysis kinetics in the focal spot) and on the diffusion of reagent (dyad) and side-product (dyads having released acetic acid) in and out of the focal spot.

Conclusions

The route toward more efficient 2P sensitive PPGs that we have explored relies on the binding, via a phosphorous clip, of a tailored 2P absorber with a caging module meant to be sensitized through energy transfer from the two-photon excited 2PA module. A small library of dyads featuring modulations of the spacer (length and nature), 2PA module and PPG (NV, NI) was successfully prepared. The comprehensive study demonstrates the modularity and versatility of this synergic strategy and reveals interesting cooperative and topological effects. In particular, the dipolar interactions between the 2PA modules and the caging moieties are found to promote cooperative effect (either negative or positive) on the 2PA response of the dyads compared to that of isolated 2PA modules. This effect is modulated by the length of the linkers as well as the nature and topology of the 2PA module. As intended, replacing the NV uncaging moiety by a more efficient one having a tenfold larger uncaging quantum yield (e.g., NI) indeed leads to much larger two-photon uncaging sensitivity. Moreover, additional contributions to the uncaging process are found to increase the global uncaging efficiency of specific MNI-derived dyads. Indeed, electron transfer seems to promote uncaging efficiency in specific cases where both the electron-donating capacity of the 2PA module and the topology of the dyad (i.e., relative positioning of the electron-donating site and NI moiety) are favorable leading to increased uncaging efficiency by 20- or 30-fold with respect to their NV-derived counterparts. When compared to the tenfold enhancement between single NV and MNI cages, this unveils interesting cooperative uncaging effects operating within NI-derived dyads.

In combination with the large 2PA response of the 2PA module bearing the stronger electron-donating end-groups, this effect leads to the measurement of two-photon uncaging cross-section values for uncaging of organic acids (i.e., up to 20 GM). This value overcomes those reported to date for the best functional uncaging systems and lies in the range of the values sought for efficient and confined photorelease of neurotransmitters (such as glutamate or GABA) in biological environments under two-photon excitation in the NIR.[50] In that respect, the excellent dark hydrolytic stability of the NI moiety and its ability to release L-glutamate on a submicrosecond time scale upon flash photolysis make such dyads very promising for further developments in the neurosciences. Building on the present results, we will thus proceed to replace caged acetic acid by neurotransmitters such as glutamate or GABA and convey solubility in physiological conditions by incorporating suitable hydro-solubilizing groups.[23,51,52] This further chemical modification will also be of major interest for direct comparison of the best synergic cages with model cages in identical conditions.

Experimental Section

Synthesis

Synthesis of D_1-C_3[Ac]: Compound **15** (23.3 mg, 78.5 μmol) and Cs_2CO_3 (102 mg, 0.31 mmol) under inert atmosphere were suspended in 3 mL of anhydrous THF. Then **8a** (27.6 mg, 71 μmol), dissolved in 2 mL of THF, was added. The reaction mixture was stirred at room temperature for 16 h. $\mathbf{M_1}$ (53 mg, 79 μmol), dissolved in 2 mL of anhydrous THF, was added and the mixture was stirred for another 18 h. The solvent was removed under reduced pressure. The crude was dissolved (partially) in CH_2Cl_2. The suspension was centrifuge-sedimented and the supernatant was evaporated. The crude was purified on silica gel (gradient eluent CH_2Cl_2/EtOAc, 1:0 to 9:1) to give **D_1-C_3[Ac]** (10 mg, 8%) as a pale yellow powder. ^{1}H NMR (300 MHz, $CDCl_3$): $\delta = 0.59$–0.71 (m, 10H), 1.03–1.15 (m, 4H), 1.95–1.99 (m, 4H), 2.16 (s, 3H), 2.23–2.33 (m, 4H), 3.30 (d, $^3J_{HP} = 10.6$ Hz, 3H), 3.84 (s, 3H), 3.85 (s, 3H), 3.93 (s, 3H), 4.09–4.18 (m, 6H), 4.26 (t, $J = 6.1$ Hz, 2H), 5.49 (s, 2H), 6.81–6.98 (m, 12H), 7.13–7.16 (m, 4H), 7.53–7.48 (m, 8H), 7.61–7.75 ppm (m, 6H); ^{13}C NMR (75 MHz, $CDCl_3$): $\delta = 14.0$, 21.0, 23.2, 26.0, 29.1, 29.4, 29.9, 33.2 (d, $^3Jcp = 13.2$ Hz, N-Me), 40.4, 55.3, 55.5, 55.5, 56.5, 63.5, 64.4, 64.6, 64.8, 66.2, 89.3, 89.9, 109.8, 111.0, 114.2, 114.4, 114.7, 115.2, 115.6, 115.7, 120.0, 122.3, 122.6, 122.6, 125.9, 127.1, 128.0, 128.6, 130.7, 133.2, 139.4, 139.6, 140.1, 140.6, 144.5, 147.7, 151.2, 154.0, 156.2, 156.3, 159.0, 159.8, 160.9, 170.5 ppm; ^{31}P NMR (121.4 MHz, $CDCl_3$): $\delta = 64.8$ ppm (s, P_0); ESIHMRS: *m/z*: calcd for $C_{75}H_{76}N_3O_{13}PS$ $[M]^+$: 1289.4836; found: 1289.4782 $[M]^+$.

Synthesis of D_1-C_6[Ac]: Compound **15** (45 mg, 0.15 mmol) and Cs_2CO_3 (197 mg, 0.6 mmol) under inert atmosphere were suspended in 3 mL of anhydrous THF. Then **8b** (65 mg, 0.15 mmol), dissolved in 2 mL of THF, was added. The reaction mixture was stirred at room temperature for 16 h. $\mathbf{M_1}$ (77 mg, 0.11 mmol), dissolved in 2 mL of anhydrous THF, was then added and the reaction mixture was stirred for another 18 h. The solvent was removed under reduced pressure. The crude was dissolved (partially) in CH_2Cl_2. The suspension was centrifuge-sedimented and the supernatant was evaporated. The crude was purified on silica gel (gradient eluent CH_2Cl_2/EtOAc, 1:0 to 9:1) to give **D_1-C_6[Ac]** (25 mg, 12%) as a pale yellow powder. ^{1}H NMR (400 MHz, $CDCl_3$): $\delta = 0.54$–0.70 (m, 10H), 1.0.3–1.16 (m, 4H), 1.53–1.55 (m, 4H), 1.77–1.92 (m, 4H), 1.96–2.01 (m, 4H), 2.16 (s, 3H), 2.23–2.27 (m, 2H), 3.30 (d, $^3J_{HP} = 10.6$ Hz, 3H), 3.85 (s, 6H), 3.91 (t, $J = 6.4$ Hz, 2H), 3.95 (s, 3H), 4.06–4.19 (m, 6H), 5.49 (s, 2H), 6.78–6.98 (m, 12H), 7.11–7.16 (m, 4H), 7.48–7.53 (m, 8H), 7.61–7.70 ppm (m, 6H); ^{13}C NMR (100 MHz, $CDCl_3$): $\delta = 14.0$, 21.0, 23.2, 25.8, 26.0, 26.0, 28.9, 29.3, 29.4, 33.3 (d, $^3J_{CP} = 12.8$ Hz), 40.4, 55.3, 55.5, 55.5, 56.5, 63.5, 64.6, 64.8, 68.2, 69.5, 89.3, 89.9, 109.5, 110.9, 114.2, 114.3, 114.7, 115.1, 115.1, 115.6, 115.6, 115.8, 116.2, 120.0, 122.3, 122.5, 122.6, 122.6, 122.6, 125.9, 126.8, 128.0, 128.6, 130.7, 133.2, 139.3, 139.5, 140.2, 140.6, 144.3 (d, $^3J_{CP} = 7.1$ Hz CH=N), 144.4, 144.5, 147.9, 151.2, 153.9, 156.3, 156.5, 159.0, 159.8, 160.9, 170.5 ppm; ^{31}P NMR (121.4 MHz, $CDCl_3$): $\delta = 64.8$ ppm (s, P_0); ESIHMRS: *m/z*: calcd for $C_{78}H_{82}N_3O_{13}PS$ $[M]^+$: 1331.5306; found: 1331.5350 $[M]^+$.

Synthesis of D_1-C_6N_3[Ac]: Compound **15** (50 mg, 0.17 mmol) and Cs_2CO_3 (219 mg, 0.67 mmol) under inert atmosphere were suspended in 5 mL of anhydrous THF. Then **6** (77 mg, 0.14 mmol), dissolved in 2 mL of THF, was added. The mixture was stirred at room temperature for 18 h. $\mathbf{M_1}$ (114 mg, 0.17 mmol), dissolved in 2 mL of anhydrous THF, was added and the reaction mixture was stirred for another 18 h. The solvent was removed under reduced pressure. The crude was dissolved (partially) in CH_2Cl_2. The suspension was centrifuge-sedimented and the supernatant was evaporated. The crude was purified on silica gel (gradient eluent CH_2Cl_2/EtOAc, 1:0

to 9:1) to give **D_1-C_6N_3[Ac]** (57 mg, 24%) as a pale yellow powder. ^{1}H NMR (300 MHz, $CDCl_3$): δ = 0.60–0.71 (m, 10H), 1.04–1.13 (m, 4H), 1.40–1.62 (m, 4H), 1.83–2.01 (m, 6H), 2.16 (s, 3H), 2.25–2.27 (m, 2H), 3.33 (t, $^3J_{HP}$ = 10.7 Hz, 3H), 3.84 (ls, 6H), 3.94 (s, 3H), 4.03–4.18 (m, 6H), 4.39 (t, $^3J_{HH}$ = 7.1 Hz, 2H), 5.49 (s, 2H), 6.82–6.98 (m, 9H), 7.15–7.18 (m, 2H), 7.28–7.31 (m, 2H), 7.48–7.52 (m, 8H), 7.62–7.69 (m, 6H), 7.76 ppm (d, $^3J_{HH}$ = 8.4 Hz, 2H); ^{13}C NMR (75 MHz, $CDCl_3$): δ = 13.9, 21.0, 23.2, 25.5, 26.0, 26.3, 28.7, 29.4, 30.3, 33.2 (d, $^3J_{CP}$ = 13.1 Hz), 40.4, 50.4, 55.2, 55.4, 56.5, 63.4, 64.6, 64.8, 69.3, 89.3, 89.8, 109.5, 110.9, 114.2, 114.3, 114.7, 115.2, 115.6, 119.4, 120.0, 122.1, 122.2, 122.3, 122.6, 125.9, 126.9, 127.9, 128.1, 128.6, 130.7, 133.2, 139.5, 139.8, 140.1, 140.6, 144.4 (d, $^3J_{CP}$ = 7.4 Hz, CH = N), 147.2, 147.8, 150.7, 151.2, 153.9, 156.3, 159.0, 159.8, 160.9, 170.5 ppm; ^{31}P NMR (121.4 MHz, $CDCl_3$): δ = 63.8 ppm (s, P_0); MALDI-TOF $C_{80}H_{83}N_6O_{12}PS$ calcd for $[M]^+$: 1383.6, found: 1383.7.

Synthesis of dyad D_3'-(C_1N_3)[Ac]: Compound **15** (30 mg, 0.1 mmol) and Cs_2CO_3 (131 mg, 0.40 mmol) under inert atmosphere were suspended in 5 mL of anhydrous THF. Then **14** (36 mg, 91 μmol), dissolved in 2 mL of THF, was added. The reaction mixture was stirred at room temperature for 18 h. **M_3** (63 mg, 91 μmol), dissolved in 2 mL of anhydrous THF, was added and the reaction mixture was heated to 40 °C and stirred for another 18 h. Then, the solvent was removed under reduced pressure. The crude was dissolved (partially) in CH_2Cl_2. The suspension was centrifuge-sedimented and the supernatant was evaporated. The crude was purified on silica gel (gradient eluent CH_2Cl_2/EtOAc, 1:0 to 9:1) to give **D_3'-(C_1N_3)[Ac]** (25 mg, 38%) as a pale yellow powder. ^{1}H NMR (600 MHz, $CDCl_3$): δ = 0.57–0.61 (m, 4H), 0.68 (t, $^3J_{HH}$ = 7.4 Hz, 6H), 1.06–1.11 (m, 4H), 1.21 (t, $^3J_{HH}$ = 7.1 Hz, 3H), 1.96–1.99 (m, 4H), 2.24 (s, 3H), 3.09 (t, $^3J_{HH}$ = 8.1 Hz, 2H), 3.33 (t, $^3J_{HP}$ = 10.7 Hz, 3H), 3.49 (q, $^3J_{HH}$ = 7.0 Hz, 2H), 3.84–3.85 (m, 6H), 4.09 (t, $^3J_{HH}$ = 8.1 Hz, 2H), 4.22 (t, $^3J_{HH}$ = 8.1 Hz, 2H), 5.37 (s, 2H), 6.68 (d, $^3J_{HH}$ = 8.8 Hz, 2H), 6.81–6.85 (m, 3H), 6.90 (d, $^3J_{HH}$ = 8.8 Hz, 2H), 6.94 (d, $^3J_{HH}$ = 8.8 Hz, 2H), 7.14–7.15 (m, 2H), 7.41–7.44 (m, 4H), 7.46–7.52 (m, 6H), 7.63–7.69 (m, 7H), 7.74 (d, $^3J_{HH}$ = 9.0 Hz, 1H), 7.96 ppm (s, 1H); ^{13}C NMR (150 MHz, $CDCl_3$): δ = 12.4, 14.0, 14.2, 22.5, 23.2, 23.5, 26.0, 26.5, 29.8, 33.2 (d, $^3J_{CP}$ = 13.1 Hz), 40.4, 45.8, 49.7, 50.5, 55.2, 55.5, 55.6, 62.4, 65.9, 88.6, 89.3, 89.8, 91.0, 107.6, 110.1, 111.6, 114.2, 114.4, 115.2, 115.6, 119.9, 120.0, 121.4, 122.0, 122.2, 122.6, 122.6, 122.9, 123.2, 123.3, 123.4, 125.6, 125.7, 125.9, 127.6, 128.6, 130.6, 130.7, 133.1, 133.2, 134.0, 135.8, 137.0, 140.1, 140.2, 140.7, 143.8, 144.3 (d, $^3J_{CP}$ = 7.1 Hz, CH = N), 147.5, 151.1, 151.3, 151.3, 156.3, 157.4, 159.8, 161.1, 168.8 ppm; ^{31}P NMR (242.8 MHz, $CDCl_3$): δ = 63.7 ppm (s, P_0); MALDI-TOF $C_{76}H_{75}N_8O_9PS$ calcd for $[M]^+$: 1306.6, found $[M+Na]^+$: 1330.5.

Synthesis of D_4-(C_3)[Ac]: Compound **15** (20.0 mg, 67 μmol) and Cs_2CO_3 (88 mg, 0.27 mmol) under inert atmosphere were suspended in 1 mL of anhydrous THF. Compound **8a** (30 mg, 76 μmol), dissolved in 3 mL of THF, was added. The mixture was stirred at room temperature for 20 h. Thereafter, the suspension was filtered and the solvent evaporated. The crude, **M_4** (48 mg, 61 μmol) and Cs_2CO_3 (88 mg, 0.27 mmol) were re-dissolved in 2 mL of anhydrous THF, and the mixture was stirred for 18 h. After completion of the reaction, the suspension was filtered and the solvent was removed under reduced pressure leading to a yellowish crude that was purified on silica gel (eluent-DCM 100%) to give **D_4-(C_3)[Ac]** (50.2 mg, 59%) as a yellow powder. ^{1}H NMR (600 MHz, $CDCl_3$): δ = 0.59–0.63 (m, 4H), 0.68 (t,$^3J_{HH}$ = 7.4 Hz, 6H), 0.97 (t,$^3J_{HH}$ = 7.4 Hz, 6H), 1.07–1.11 (m, 4H), 1.21 (t,$^3J_{HH}$ = 7.1 Hz, 3H), 1.34–1.40 (m, 4H), 1.56–1.61 (m, 4H), 1.96–1.99 (m, 4H), 2.16 (s, 3H), 2.29–2.33 (m, 2H), 3.28–3.31 (m, 7H), 3.49 (q,$^3J_{HH}$ = 7.1 Hz, 2H), 3.73 (t,$^3J_{HH}$ = 6.0 Hz, 2H), 3.84 (s, 3H), 3.93 (s, 3H), 4.07 (t,$^3J_{HH}$ = 6.1 Hz, 2H),4.12 (t,$^3J_{HH}$ = 5.9 Hz, 2H), 4.26 (t,$^3J_{HH}$ = 6.2 Hz, 2H), 5.49 (s, 1H), 6.60 (d,$^3J_{HH}$ = 9.1 Hz, 2H),6.67 (d, $^3J_{HH}$ = 9.1 Hz, 2H),6.79–6.84 (m, 4H), 6.94 (d, $^3J_{HH}$ = 8.8 Hz, 2H), 6.98 (s, 1H), 7.13–7.15 (m, 4H), 7.40–7.49 (m, 8H), 7.61–7.63 (m, 3H),7.69 (d, $^3J_{HH}$ = 8.8 Hz, 2H), 7.78 ppm (s, 1H); ^{13}C NMR (150 MHz, $CDCl_3$): δ = 12.4, 14.0, 14.1, 20.5, 21.0, 23.2, 26.0, 29.0, 29.5, 33.1 (d, $^3J_{CP}$ = 12.8 Hz), 40.4, 45.8, 49.7, 50.8, 55.2, 55.5, 56.4, 63.4, 64.4, 65.8, 66.1, 88.3, 88.6, 90.9, 91.3, 108.8, 109.8, 110.0, 110.9, 111.3, 111.5, 114.3, 115.1, 119.8, 122.6 (m), 122.9, 125.6, 125.7, 127.1, 127.9, 128.6, 130.5, 133.0, 133.1, 139.4, 139.5, 140.1, 140.3, 144.4 (d, $^3J_{CP}$ = 7.0 Hz, CH = N), 147.5, 147.7, 148.1, 151.0, 153.9, 156.1, 156.2, 160.8, 170.4 ppm; ^{31}P NMR (121.4 MHz, $CDCl_3$): δ = 64.7 ppm (s, P_0); MALDI-TOF $C_{83}H_{94}N_5O_{11}PS$ calcd for $[M]^+$: 1399.6, found $[M+K]^+$: 1438.4.

Synthesis of D_4'-(C_1N_3)[Ac]: Compound **15** (22.5 mg, 76 μmol) and Cs_2CO_3 (99 mg, 0.30 mmol) under inert atmosphere were suspended in 1 mL of anhydrous THF. Compound **14** (30 mg, 76 μmol), dissolved in 4 mL of THF, was added. The mixture was stirred at room temperature for 6 h. Thereafter, the suspension was filtered and the solvent was evaporated. The crude, **M_4** (54 mg, 68 μmol) and Cs_2CO_3 (99 mg, 0.30 mmol) were re-dissolved in 2 mL of anhydrous THF, and the mixture was stirred for 18 h. After completion of the reaction, the suspension was filtered and the solvent was removed under reduced pressure leading to a yellowish crude that was purified on silica gel (gradient eluent CH_2Cl_2/AcOEt, 1:0 to 9:1) to give **D_4'-(C_1N_3)[Ac]** (25 mg, 23%) as a brownish powder. ^{1}H NMR (600 MHz, $CDCl_3$): δ = 0.53–0.63 (m, 4H), 0.67 (t, $^3J_{HH}$ = 7.3 Hz, 6H), 0.97 (t, $^3J_{HH}$ = 7.4 Hz, 6H), 1.07–1.11 (m, 4H), 1.21 (t, $^3J_{HH}$ = 7.0 Hz, 3H),1.34–1.39 (m, 4H), 1.54–1.63 (m, 4H), 1.94–1.99 (m, 4H), 2.23 (s, 3H), 3.09 (t, $^3J_{HH}$ = 7.9 Hz, 2H), 3.26–3.35 (m, 7H), 3.45–3.52 (m, 2H), 3.73 (t,$^3J_{HH}$ = 5.7 Hz, 2H),3.84 (s, 3H), 4.08 (t, $^3J_{HH}$ = 5.9 Hz, 2H), 4.21 (t, $^3J_{HH}$ = 8.1 Hz, 2H), 5.36 (s, 2H),6,59 (d, $^3J_{HH}$ = 8.8 Hz, 2H), 6,67 (d, $^3J_{HH}$ = 8.7 Hz, 2H), 6.81–6.85 (m, 3H), 6.94 (d, $^3J_{HH}$ = 8.6 Hz, 2H), 7.15 (d, $^3J_{HP}$ = 8.1 Hz, 2H), 7.39–7.48 (m, 10H), 7.61–7.68 (m, 7H), 7.74 (d, $^3J_{HP}$ = 9.0 Hz, 1H), 7.96 ppm (s, 1H); ^{13}C NMR (150 MHz, $CDCl_3$): δ = 12.4, 14.0, 14.2, 20.5, 23.2, 23.5, 26.0, 26.5, 29.5, 29.8, 33.2 (d, $^3J_{CP}$ = 13.1 Hz), 40.5, 45.8, 49.7, 50.5, 50.8, 55.2, 55.5, 62.4, 65.9, 88.3, 88.6, 90.9, 91.4, 107.6, 108.9, 110.1, 111.4, 111.6, 114.4, 115.2, 119.8, 121.4, 122.0, 122.6, 123.0, 123.2 (2 s), 123.4, 125.6, 125.7 (2 s), 127.6, 128.6, 130.5, 133.0, 134.0, 135.8, 137.0, 140.1 (2 s), 140.2, 140.4, 143.8, 144.3 (d, $^3J_{CP}$ = 6.9 Hz), 147.5, 148.1, 151.0, 151.2, 156.3, 157.4, 161.1, 168.8 ppm; ^{31}P NMR (121.4 MHz, $CDCl_3$): δ = 63.7 ppm (s, P_0); MALDI-TOF $C_{83}H_{90}N_9O_8PS$ calcd for $[M]^+$: 1403.6, found $[M]^+$: 1403.8.

Photophysical studies and photolysis experiments

All photophysical studies were performed with freshly prepared air-equilibrated solutions at room temperature (298 K). UV/Vis absorption spectra of 10^{-5} M solutions were recorded on a Jasco V-670 spectrophotometer. Steady-state fluorescence measurements were performed on dilute solutions (ca. 10^{-6} M, optical density <0.1) contained in standard 1 cm quartz cuvettes by using a Fluorolog spectro fluorometer. Emission spectra were obtained, for each compound, under excitation at the wavelength of the absorption maximum. Fluorescence quantum yields were measured according to literature procedures.

2PA cross-sections (σ_2) were derived from the two-photon excited fluorescence (TPEF) cross-sections ($\sigma_2\Phi_f$) and the fluorescence emission quantum yield (Φ_f). TPEF cross-sections were measured relative to fluorescein in 0.01 M aqueous NaOH,[53] using the well-established method described by Xu and Webb[54] and the appropriate solvent-related refractive index corrections.[55] The quadratic dependence of the fluorescence intensity on the excitation power was checked for each sample and all wavelengths. Measurements were conducted using an excitation source delivering fs pulses. A

Chameleon Ultra II (Coherent) was used generating 140 fs pulses at an 80 MHz repetition rate. The excitation was focused into the cuvette through a microscope objective (10×, NA 0.25). The fluorescence was detected in epifluorescence mode with a dichroic mirror (Chroma 675dcxru) and a barrier filter (Chroma e650sp-2p) by a compact CCD spectrometer module BWTek BTC112E. Total fluorescence intensities were obtained by integrating the corrected emission.

The one-photon uncaging sensitivity of dyads was determined by irradiating solutions of dyads and NVOAc or MNI (used as standards for **D_1-D_4** and **D_2'-D_4'** dyads, respectively) having the same absorbance at 365 nm. The solutions (0.6 mL) prepared in $CDCl_3$ were introduced in a quartz NMR tube which was irradiated with three UV-lamps (VilberLourmat, Model VL-6.LC) arranged in a triangular configuration. The conversion rate (X) was monitored over time by ^{1}H NMR spectroscopy by following the decrease of the singlet at 2.16 or 2.23 ppm (corresponding to caged acetyl CH_3-COOR), in the case of NV and MNI-based dyads respectively, and onset of the singlet at 2.10 ppm (corresponding to released acetic acid). A first order kinetics was observed for all derivatives. Comparison of the conversion kinetics for dyads and reference PPG (i.e., NVOAc or MNI) allowed to calculate the $\varepsilon_{365}Q_u$(dyad)/$\varepsilon_{365}Q_u$ (NVOAc) ratio values for **D_1-D_4** dyads and $\varepsilon_{365}Q_u$(dyad)/$\varepsilon_{365}Q_u$ (MNI) ratio values for **D_2'-D_4'** dyads. Using ε_{365} values derived from the absorption spectra, the ratio values (Q_u(dyad)/Q_u (NV) for **D_1-D_4** dyads and Q_u(dyad)/Q_u (MNI) or **D_2'-D_4'** dyads) could be calculated.

Acknowledgements

This work has been supported by funding from the European Community's Seventh Framework Program under TOPBIO project-grant agreement no. 264362. M.B.D. thanks the Conseil Régional d'Aquitaine for funding (Chaire d'Accueil grant and fellowship to V.H.). We also acknowledge financial support from Agence Nationale pour la Recherche (Grant 2010 ANR-10-BLAN-1436) and University of Bordeaux for a fellowship to M.K. This work also received funding from the People Programme (Marie Curie Actions) of the European Union's Seventh Framework Programme FP7/2007-2013/ under REA grant agreement number 607721 (fellowship to P.P.). The authors are grateful to Jean-Pierre Majoral for generous gift of MMH-$PSCl_2$.

Keywords: caged compounds · Förster resonance energy transfer · photolysis · two-photon absorption · two-photon uncaging

[1] J. A. Barltrop, P. Schofield, *Tetrahedron Lett.* **1962**, *3*, 697 – 699.
[2] J. Engels, E. J. Schlaeger, *J. Med. Chem.* **1977**, *20*, 907 – 911.
[3] J. H. Kaplan, B. Forbush, J. F. Hoffman, *Biochemistry (Mosc.)* **1978**, *17*, 1929 – 1935.
[4] V. N. Rajasekharan Pillai, *Synthesis* **1980**, *1980*, 1 – 26.
[5] Z. Li, W. E. Lee, W. C. Galley, *Biophys. J.* **1989**, *56*, 361 – 367.
[6] C. G. Bochet, *J. Chem. Soc. Perkin Trans. 1* **2002**, 125 – 142.
[7] P. Klán, T. Šolomek, C. G. Bochet, A. Blanc, R. Givens, M. Rubina, V. Popik, A. Kostikov, J. Wirz, *Chem. Rev.* **2013**, *113*, 119 – 191.
[8] C. Brieke, F. Rohrbach, A. Gottschalk, G. Mayer, A. Heckel, *Angew. Chem. Int. Ed.* **2012**, *51*, 8446 – 8476; *Angew. Chem.* **2012**, *124*, 8572 – 8604.
[9] H. Yu, J. Li, D. Wu, Z. Qiu, Y. Zhang, *Chem. Soc. Rev.* **2010**, *39*, 464 – 473.
[10] W. Lu, C. Tian, P. Thogaripally, J. Hu, P. Wang, *Chem. Commun.* **2013**, *49*, 9636 – 9638.
[11] K. A. Mosiewicz, L. Kolb, A. J. van der Vlies, M. P. Lutolf, *Biomater. Sci.* **2014**, *2*, 1640 – 1651.
[12] A. Banerjee, C. Grewer, L. Ramakrishnan, J. Jäger, A. Gameiro, H.-G. A. Breitinger, K. R. Gee, B. K. Carpenter, G. P. Hess, *J. Org. Chem.* **2003**, *68*, 8361 – 8367.
[13] G. C. R. Ellis-Davies, *Nat. Methods* **2007**, *4*, 619 – 628.
[14] A. C. Rea, L. N. Vandenberg, R. E. Ball, A. A. Snouffer, A. G. Hudson, Y. Zhu, D. E. McLain, L. L. Johnston, J. D. Lauderdale, M. Levin, *Chem. Biol.* **2013**, *20*, 1536 – 1546.
[15] L. Fournier, C. Gauron, L. Xu, I. Aujard, T. Le Saux, N. Gagey-Eilstein, S. Maurin, S. Dubruille, J.-B. Baudin, D. Bensimon, *ACS Chem. Biol.* **2013**, *8*, 1528 – 1536.
[16] D. E. McLain, A. C. Rea, M. B. Widegren, T. M. Dore, *Photochem. Photobiol. Sci.* **2015**, *14*, 2151 – 2158.
[17] R. Horbert, B. Pinchuk, P. Davies, D. Alessi, C. Peifer, *ACS Chem. Biol.* **2015**, *10*, 2099 – 2107.
[18] W. Denk, J. Strickler, W. Webb, *Science* **1990**, *248*, 73 – 76.
[19] W. R. Zipfel, R. M. Williams, W. W. Webb, *Nat. Biotechnol.* **2003**, *21*, 1369 – 1377.
[20] G. Bort, T. Gallavardin, D. Ogden, P. I. Dalko, *Angew. Chem. Int. Ed.* **2013**, *52*, 4526 – 4537; *Angew. Chem.* **2013**, *125*, 4622 – 4634.
[21] N. Gagey, P. Neveu, L. Jullien, *Angew. Chem. Int. Ed.* **2007**, *46*, 2467 – 2469; *Angew. Chem.* **2007**, *119*, 2519 – 2521.
[22] L. Donato, A. Mourot, C. M. Davenport, C. Herbivo, D. Warther, J. Léonard, F. Bolze, J.-F. Nicoud, R. H. Kramer, M. Goeldner, *Angew. Chem. Int. Ed.* **2012**, *51*, 1840 – 1843; *Angew. Chem.* **2012**, *124*, 1876 – 1879.
[23] G. C. R. Ellis-Davies, J. M. Amatrudo, J. P. Olson, G. Lur, C. Q. Chiu, M. J. Higley, *ACS Chem. Neurosci.* **2014**, *5*, 64 – 70.
[24] C. Tran, T. Gallavardin, M. Petit, R. Slimi, H. Dhimane, M. Blanchard-Desce, F. C. Acher, D. Ogden, P. I. Dalko, *Org. Lett.* **2015**, *17*, 402 – 405.
[25] N. Komori, S. Jakkampudi, R. Motoishi, M. Abe, K. Kamada, K. Furukawa, C. Katan, W. Sawada, N. Takahashi, H. Kasai, *Chem. Commun.* **2015**, *51*, 331 – 334.
[26] S. Gug, F. Bolze, A. Specht, C. Bourgogne, M. Goeldner, J.-F. Nicoud, *Angew. Chem. Int. Ed.* **2008**, *47*, 9525 – 9529.
[27] P. Dunkel, C. Tran, T. Gallavardin, H. Dhimane, D. Ogden, P. I. Dalko, *Org. Biomol. Chem.* **2014**, *12*, 9899 – 9908.
[28] H. K. Agarwal, R. Janicek, S.-H. Chi, J. W. Perry, E. Niggli, G. C. R. Ellis-Davies, *J. Am. Chem. Soc.* **2016**, *138*, 3687 – 3693.
[29] S. Picard, E. Genin, G. Clermont, V. Hugues, O. Mongin, M. Blanchard-Desce, *New J. Chem.* **2013**, *37*, 3899 – 3913.
[30] I. Aujard, C. Benbrahim, M. Gouget, O. Ruel, J.-B. Baudin, P. Neveu, L. Jullien, *Chem. Eur. J.* **2006**, *12*, 6865 – 6879.
[31] S. Gug, S. Charon, A. Specht, K. Alarcon, D. Ogden, B. Zietz, J. Léonard, S. Haacke, F. Bolze, J.-F. Nicoud, *ChemBioChem* **2008**, *9*, 1303 – 1307.
[32] S. Picard, E. J. Cueto-Diaz, E. Genin, G. Clermont, F. Acher, D. Ogden, M. Blanchard-Desce, *Chem. Commun.* **2013**, *49*, 10805 – 10807.
[33] K. A. Korzycka, P. M. Bennett, E. J. Cueto-Diaz, G. Wicks, M. Drobizhev, M. Blanchard-Desce, A. Rebane, H. L. Anderson, *Chem. Sci.* **2015**, *6*, 2419 – 2426.
[34] E. J. Cueto Díaz, S. Picard, V. Chevasson, J. Daniel, V. Hugues, O. Mongin, E. Genin, M. Blanchard-Desce, *Org. Lett.* **2015**, *17*, 102 – 105.
[35] M. Canepari, G. Papageorgiou, J. E. T. Corrie, C. Watkins, D. Ogden, *J. Physiol.* **2001**, *533*, 765 – 772.
[36] M. Canepari, L. Nelson, G. Papageorgiou, J. E. Corrie, D. Ogden, *J. Neurosci. Methods* **2001**, *112*, 29 – 42.
[37] G. Lowe, *J. Neurophysiol.* **2003**, *90*, 1737 – 1746.
[38] M. Matsuzaki, G. C. R. Ellis-Davies, T. Nemoto, Y. Miyashita, M. Iino, H. Kasai, *Nat. Neurosci.* **2001**, *4*, 1086 – 1092.
[39] T. Furuta, S. S.-H. Wang, J. L. Dantzker, T. M. Dore, W. J. Bybee, E. M. Callaway, W. Denk, R. Y. Tsien, *Proc. Natl. Acad. Sci. USA* **1999**, *96*, 1193 – 1200.
[40] J. Corrie, G. Papageorgiou, *7-Nitroindoline Derivatives and Their Uses* **2004**, WO2004085394 (A1).
[41] Q. Cai, W. Zhu, H. Zhang, Y. Zhang, D. Ma, *Synthesis* **2005**, *2005*, 496 – 499.
[42] O. Mongin, T. R. Krishna, M. H. V. Werts, A.-M. Caminade, J.-P. Majoral, M. Blanchard-Desce, *Chem. Commun.* **2006**, 915 – 917.
[43] C. Rouxel, M. Charlot, O. Mongin, T. R. Krishna, A.-M. Caminade, J.-P. Majoral, M. Blanchard-Desce, *Chem. Eur. J.* **2012**, *18*, 16450 – 16462.
[44] C. Katan, M. Charlot, O. Mongin, C. Le Droumaguet, V. Jouikov, F. Terenziani, E. Badaeva, S. Tretiak, M. Blanchard-Desce, *J. Phys. Chem. B* **2010**, *114*, 3152 – 3169.

[45] D. L. Andrews, J. S. Ford, *J. Chem. Phys.* **2013**, *139*, 014107.
[46] F. Terenziani, M. Morone, S. Gmouh, M. Blanchard-Desce, *ChemPhysChem* **2006**, *7*, 685 – 696.
[47] G. Papageorgiou, M. Lukeman, P. Wan, J. E. T. Corrie, *Photochem. Photobiol. Sci.* **2004**, *3*, 366 – 373.
[48] K. Lee, D. E. Falvey, *J. Am. Chem. Soc.* **2000**, *122*, 9361 – 9366.
[49] D. E. Falvey, C. Sundararajan, *Photochem. Photobiol. Sci.* **2004**, *3*, 831 – 838.
[50] N. I. Kiskin, R. Chillingworth, J. A. McCray, D. Piston, D. Ogden, *Eur. Biophys. J.* **2002**, *30*, 588 – 604.
[51] G. Papageorgiou, D. Ogden, J. E. T. Corrie, *Photochem. Photobiol. Sci.* **2008**, *7*, 423 – 432.
[52] G. C. R. Ellis-Davies, M. Matsuzaki, M. Paukert, H. Kasai, D. E. Bergles, *J. Neurosci.* **2007**, *27*, 6601 – 6604.
[53] M. A. Albota, C. Xu, W. W. Webb, *Appl. Opt.* **1998**, *37*, 7352.
[54] C. Xu, W. W. Webb, *J. Opt. Soc. Am. B* **1996**, *13*, 481.
[55] M. H. V. Werts, N. Nerambourg, D. Pélégry, Y. L. Grand, M. Blanchard-Desce, *Photochem. Photobiol. Sci.* **2005**, *4*, 531 – 538.

Received: March 8, 2016
Revised: May 19, 2016
Published online on June 27, 2016